
OPERATOR-INFORMED SCORE MATCHING FOR MARKOV DIFFUSION MODELS

Zheyang Shen
Newcastle University, UK
zheyang.shen@ncl.ac.uk

Chris J. Oates
Newcastle University, UK
Alan Turing Institute, UK
chris.oates@ncl.ac.uk

ABSTRACT

Diffusion models are typically trained using score matching, yet score matching is agnostic to the particular forward process that defines the model. This paper argues that *Markov* diffusion models enjoy an advantage over other types of diffusion model, as their associated operators can be exploited to improve the training process. In particular, (i) there exists an *explicit* formal solution to the forward process as a sequence of time-dependent kernel mean embeddings; and (ii) the derivation of score-matching and related estimators can be streamlined. Building upon (i), we propose *Riemannian diffusion kernel smoothing*, which ameliorates the need for neural score approximation, at least in the low-dimensional context, and building upon (ii), we propose *operator-informed score matching*, a variance reduction technique that is straight-forward to implement in both low- and high-dimensional diffusion modeling and is demonstrated to improve score matching in an empirical proof-of-concept.

Keywords Forward process · Markov semigroup · score matching

Diffusion models (DMs) (Sohl-Dickstein et al., 2015; Song and Ermon, 2019; Ho et al., 2020) have demonstrated remarkable performance in generative modeling, including in many instances where data are complicated and high-dimensional. Their conceptual appeal stems from the simple yet illuminating observation that “creating noise from data is easy” (Song et al., 2020), as myriad tractable diffusion processes (often known as *forward processes*) can be used to evolve a hard-to-sample data distribution p_{data} into an easy-to-sample noise distribution π . The forward process induces a corresponding *backward process*, whose law coincides with the “time reversal” of the forward process and can be approximated using techniques such as score matching (Hyvärinen, 2005). Simulation of the backward process enables samples from p_{data} to be approximately generated. Markov DMs in particular have been shown to provide state-of-the-art performance on tasks such as image generation (Rombach et al., 2022), text-to-3D (Poole et al., 2022), and prediction of molecular binding structure (Corso et al., 2023).

Practically, the forward process plays a supporting role of degrading structured data into unstructured noise, and considerable flexibility exists for how noise is incorporated within a DM; for example, it is not required that the forward process is Markov, or even a diffusion process (despite the DM terminology) (Bansal et al., 2023). Regardless of how the forward process is specified, accurate approximation of the noise-perturbed score functions is critical, and this is typically achieved using generic estimation techniques, such as score matching applied to a sufficiently large dataset. However, while any continuous-time forward process can be inverted using an accurate approximations to the score functions, the aim of this paper is to demonstrate that *Markov* forward processes offer important additional new insight and functionality for a DM:

- **Exact solution of the forward process:** A Markov forward process has a formal solution as a sequence of time-dependent kernel mean embeddings (KMEs) of the data-generating distribution (Smola et al., 2007), meaning that in principle both forward and backward processes can be *exactly solved*. Though in practice the data-generating distribution is not directly observed, this insight enables the development of a novel technique called *Riemannian diffusion kernel smoothing*, which can ameliorate the burden of neural score approximation for DM, at least in a low-dimensional context.
- **New insight into score matching:** Self-adjointness of diffusion operators streamlines the derivation of tractable formula for score matching, and by extension, the L_2 minimization of the conditional expectation of any functional.

Streamlined derivations for time score matching (Choi et al., 2022) and the score Fokker–Planck equation (Lai et al., 2023a) can also be obtained.

- **Improved score matching:** For Markov DMs we propose *operator-informed score matching*; a novel, widely applicable, and straight-forward to implement approach to score matching that exploits an explicitly computable low-order approximation to the score function. This has the effect of reducing sample complexity, and is demonstrated to lead to more precise estimates in an empirical proof-of-concept.

Coupling the score matching methodology to the choice of forward process is a relatively unexplored direction in DM. The recent work of Scarvelis et al. (2023); Lai et al. (2023a) proposed different and more practical perspectives on this issue compared to the present paper, as discussed in detail in Section 5. Our principal contributions are theoretical, and we adopt the framework of *Markov diffusion operators* as coined by Bakry et al. (2013). Markov diffusion operators present an aerial view of the corresponding forward process as an evolution of laws guided by Markov semi-group operators, and we contend that this perspective enables useful insights, as well as the development of improved methodology, in the context of DMs.

The set-up and notation used in this paper is introduced in Section 1. Our principal insights into DMs are obtained through the lens of Markov diffusion operators in Section 2. Consequences of an explicit closed form solution to the forward process are explored in Section 3, while the proposed operator-informed score matching methodology is presented in Section 4. An extended discussion is contained in Section 5.

1 Set-up and Notation

Given a set $\{\mathbf{x}_n\}_{n=1}^N$ of independent samples from p_{data} , the task is to construct a *generative model*, meaning an accurate approximation to p_{data} that can be easily sampled. For concreteness we suppose in this paper that p_{data} is supported on \mathbb{R}^d , and for convenience we overload notation so that (e.g.) p_{data} refers both to the distribution and its associated density on \mathbb{R}^d . Similarly we let $\mathcal{N}(\boldsymbol{\mu}, \boldsymbol{\Sigma})$ denote the Gaussian distribution with mean $\boldsymbol{\mu} \in \mathbb{R}^d$ and covariance $\boldsymbol{\Sigma} \in \mathbb{R}^{d \times d}$, and we let $\mathcal{N}(\cdot | \boldsymbol{\mu}, \boldsymbol{\Sigma})$ denote the corresponding density function in shorthand.

The generative models we consider are DMs, and these will now be briefly described. The *forward process* of a DM is a stochastic process $(\mathbf{X}_t)_{t \geq 0}$ whose initial point $\mathbf{X}_0 \in \mathbb{R}^d$ is sampled from $\rho_0 := p_{\text{data}}$, the law which gives rise to the dataset, and for which the law ρ_t of subsequent states \mathbf{X}_t converges to an explicitly known noise distribution π in the $t \rightarrow \infty$ limit. Prominent examples include the *variance-exploding DM*

$$d\mathbf{X}_t = d\mathbf{W}_t, \quad \mathbf{X}_0 \sim p_{\text{data}}, \quad (1)$$

where \mathbf{W}_t denotes a standard d -dimensional Brownian motion (BM), and the *variance-preserving DM*

$$d\mathbf{X}_t = -\mathbf{X}_t dt + \sqrt{2} d\mathbf{W}_t, \quad \mathbf{X}_0 \sim p_{\text{data}}, \quad (2)$$

which is recognised as an Ornstein–Uhlenbeck (OU) process (Song et al., 2020). In the case of the OU process, it is well-known that the marginal distribution ρ_t converges to the standard Gaussian distribution $\pi = \mathcal{N}(\mathbf{0}, \mathbf{I})$ as $t \rightarrow \infty$, and that the distribution $\rho_t(\mathbf{X}_t | \mathbf{X}_0)$ of \mathbf{X}_t conditioned the initial point \mathbf{X}_0 , is equal to $\mathcal{N}(\mathbf{X}_t | \alpha_t \mathbf{X}_0, \sigma_t^2 \mathbf{I})$, where $\alpha_t := e^{-t}$, $\sigma_t^2 := 1 - \alpha_t^2$. In practice, the forward process is run until a finite time horizon T , big enough such that $\rho_T \approx \pi$. The *probability flow* ordinary differential equation (ODE) (Song et al., 2020)

$$\frac{d\mathbf{X}_t}{dt} = -\nabla \log \frac{\rho_t}{\pi}(\mathbf{X}_t) = -\mathbf{X}_t - \nabla \log \rho_t(\mathbf{X}_t) \quad (3)$$

describes the evolution of the marginal distributions ρ_t under the OU dynamics. The main observation in DM is that simulating (3) backwards in time (the *backwards process*) with initialization $\mathbf{X}_T \sim \pi$ approximately yields $\mathbf{X}_0 \sim \rho_0$. To instantiate the backwards process, the score of ρ_t , i.e., $\nabla \log \rho_t(\mathbf{x})$, must be estimated (Hyvärinen, 2005; Vincent, 2011).

For the purposes of this paper we assume all relevant densities exist and are positive and differentiable as required, and that all integrals we consider exist. Our aim is not to provide a rigorous mathematical treatment, but we note that excellent introductions to the mathematical tools of DM can be found in Øksendal (2003); Stroock (2013); Särkkä and Solin (2019).

Markov diffusion processes, as typified by the OU process in (2), remain the default choice for DM. However, any forward process yielding a time-indexed distribution sequence of decreasing complexity can in principle be inverted in time, once quantities of the intermediate distributions are accurately approximated (Bansal et al., 2023). This paper presents new theoretical insight that highlights particular advantages of Markov diffusion processes, relative to other possible choices of forward process, in the context of DMs. To achieve this, we revisit DM through the lens of Markov diffusion operators, next.

2 Diffusion Models Through the Lens of Markov Diffusion Operators

This section sets out our novel theoretical insight into Markov DMs. Our main tools are Markov diffusion operators (Bakry et al., 2013), a family of operators that can be used to characterize the marginal distributions $(\rho_t)_{t \geq 0}$ of a Markov DM (Section 2.1). These operators are demonstrated to enable exact solution of the forward process (Section 2.2), and exploited to shed new light on score matching and related objectives (Section 2.3).

2.1 Spectral Properties of Markov Diffusion Forward Processes

One of the fundamental ideas that we exploit in this paper is that the convergence of a Markov diffusion process to its stationary distribution π can be characterized from the perspective of its Markov semigroup and infinitesimal generator, as will now be explained. The *Markov semigroup* $(P_t)_{t \geq 0}$ is a family of operators such that $P_t f(\mathbf{x})$ evaluates the conditional expected value of $f(\mathbf{X}_t)$ with \mathbf{X}_0 initialized at \mathbf{x} , i.e.,

$$P_t f(\mathbf{x}) := \mathbb{E}_{\mathbf{X}_t \sim \rho_t(\mathbf{x}_t | \mathbf{x}_0 = \mathbf{x})} [f(\mathbf{X}_t)].$$

Moreover, we can denote $(P_t)_{t \geq 0}$ more parsimoniously using its *infinitesimal generator* that measures the infinitesimal change in a quantity $f(\mathbf{x})$ as time is evolved:

$$\mathcal{L}f(\mathbf{x}) := \lim_{t \downarrow 0} \frac{P_t f(\mathbf{x}) - f(\mathbf{x})}{t}$$

Specifically, we can formally express P_t as $e^{t\mathcal{L}}$, where the exponential of an operator is defined by the Taylor expansion of the exponential function. Since a stationary measure π of a Markov diffusion processes satisfies $\mathbb{E}_{\mathbf{X} \sim \pi} [P_t f(\mathbf{X})] = \mathbb{E}_{\mathbf{X} \sim \pi} [f(\mathbf{X})]$, it follows that the range of \mathcal{L} contains only functions whose expectations are zero with respect to π .

Example 1 (BM process) *The Markov semigroup associated with the BM process in (1) is $P_t f(\mathbf{x}) = \mathbb{E}_{\mathbf{X}_t \sim \mathcal{N}(\alpha_t \mathbf{x}, \sigma_t^2 \mathbf{I})} f(\mathbf{X}_t)$, where $\alpha_t = 1$ and $\sigma_t^2 = t$ and the infinitesimal generator is $\mathcal{L}f(\mathbf{x}) = \Delta f(\mathbf{x})$; see Example 7.3.4 of Øksendal (2003).*

Example 2 (OU process) *The Markov semigroup associated with the OU process in (2) is $P_t f(\mathbf{x}) = \mathbb{E}_{\mathbf{X}_t \sim \mathcal{N}(\alpha_t \mathbf{x}, \sigma_t^2 \mathbf{I})} f(\mathbf{X}_t)$, where $\alpha_t = e^{-t}$, $\sigma_t^2 = 1 - \alpha_t^2$, and the infinitesimal generator is $\mathcal{L}f(\mathbf{x}) = \langle -\mathbf{x}, \nabla f(\mathbf{x}) \rangle + \Delta f(\mathbf{x})$; see Theorem 7.3.3 of Øksendal (2003).*

Further examples include e.g. the critically-damped OU process (Dockhorn et al., 2021). To improve presentation we will principally focus on the OU forward process in the sequel, but our derivations can be reproduced for other Markov diffusion processes: we include a general derivation for most linear time-invariant (LTI) stochastic differential equations (SDEs) (Särkkä and Solin, 2019) in Appendix A.

Armed with the concept of an infinitesimal generator, we can now define the *spectrum* of a Markov diffusion process as consisting of eigenpairs $(\lambda_n, \phi_n)_{n \geq 0}$ of the infinitesimal generator, such that $\mathcal{L}\phi_n(\mathbf{x}) = \lambda_n \phi_n(\mathbf{x})$. The spectrum of the Markov semigroup can be similarly defined as consisting of pairs $(e^{\lambda_n t}, \phi_n)_{n \geq 0}$, which satisfy the eigen-relation

$$\mathbb{E}_{\mathbf{X}_t \sim \rho_t} [\phi_n(\mathbf{X}_t)] = \mathbb{E}_{\mathbf{X}_0 \sim \rho_0} [P_t \phi_n(\mathbf{X}_0)] = e^{\lambda_n t} \mathbb{E}_{\mathbf{X}_0 \sim \rho_0} [\phi_n(\mathbf{X}_0)], \quad (4)$$

meaning that the moments of the eigenfunctions ϕ_n evolve in a predictable way under the OU dynamics as governed by the exponent λ_n in (4).

Example 3 (OU process, continued) *In the one-dimensional setting ($d = 1$), the OU process has spectrum consisting of eigenpairs $(\lambda_n, \phi_n)_{n \geq 0}$ with $\lambda_n = -n$ and $\phi_n(x) = \text{He}_n(x)/\sqrt{n!}$, with $\text{He}_n(x)$ the n th probabilist's Hermite polynomial. In the multivariate setting ($d > 1$) the eigenpairs become tensorized as sums $\lambda_{n_1} + \dots + \lambda_{n_d}$ and products $\phi_{n_1}(x_1) \dots \phi_{n_d}(x_d)$ of the one-dimensional eigenpairs, indexed by $\{(n_1, \dots, n_d) : n_1, \dots, n_d \geq 0\}$. In each case, the eigenfunctions form an orthogonal basis for $L^2(\pi)$; see Section 2.7.1. of Bakry et al. (2013).*

2.2 Exact Solution of the Forward Process

The first main insight that we present is that the sequence of distributions $(\rho_t)_{t \geq 0}$ produced under a linear Markov diffusion forward process can be *explicitly* characterised as a sequence of kernel mean embeddings of the data-generating distribution.

The Markov semigroup in the case of a linear SDE takes the explicit form of an integral operator

$$P_t f(\mathbf{x}) = \int \mathcal{N}(\tilde{\mathbf{x}}|\alpha_t \mathbf{x}, \sigma_t^2 \mathbf{I}) f(\tilde{\mathbf{x}}) d\tilde{\mathbf{x}} = \int k_t(\mathbf{x}, \tilde{\mathbf{x}}) f(\tilde{\mathbf{x}}) d\pi(\tilde{\mathbf{x}}), \quad (5)$$

with the values of α_t and σ_t depending on the SDE (c.f. Examples 1 and 2). It is conventional to describe the Markov semigroup as an integral operator with respect to the Lebesgue measure, but by writing it instead as an integral operator with respect to π in (5) we obtain a *kernel integral operator* with symmetric positive definite *kernel* $k_t : \mathbb{R}^d \times \mathbb{R}^d \rightarrow \mathbb{R}$. In the case of the OU process, π is a standard Gaussian distribution and the kernel takes the explicit form

$$k_t(\mathbf{x}, \tilde{\mathbf{x}}) = \frac{1}{\sigma_t^d} \exp\left(-\frac{\alpha_t^2 \|\mathbf{x}\|^2 + \alpha_t^2 \|\tilde{\mathbf{x}}\|^2 - 2\alpha_t \langle \mathbf{x}, \tilde{\mathbf{x}} \rangle}{2\sigma_t^2}\right) = \frac{\rho_t(\tilde{\mathbf{x}}|\mathbf{x})}{\pi(\tilde{\mathbf{x}})}, \quad (6)$$

which is recognized as an instance of the *Mehler kernel* (Mehler, 1866). It is straightforward to verify that the Mehler kernels are positive definite for any $t > 0$, although its behavior as $t \downarrow 0$ becomes pathological. For convenience we will adopt the shorthand ρ_t/π for the function $\mathbf{x} \mapsto \rho_t(\mathbf{x})/\pi(\mathbf{x})$. As k_t can also be represented as both the Mehler kernel and the density ratio between the conditional density $\rho_t(\tilde{\mathbf{x}}|\mathbf{x})$ and $\pi(\tilde{\mathbf{x}})$, we arrive at the following *explicit* representation of ρ_t in terms of the density ratio ρ_t/π :

$$\frac{\rho_t}{\pi}(\tilde{\mathbf{x}}) = \frac{\int \rho_t(\tilde{\mathbf{x}}|\mathbf{x}) d\rho_0(\mathbf{x})}{\pi(\tilde{\mathbf{x}})} = \int k_t(\mathbf{x}, \tilde{\mathbf{x}}) d\rho_0(\mathbf{x}) = \int k_t(\mathbf{x}, \tilde{\mathbf{x}}) \frac{\rho_0(\mathbf{x})}{\pi(\mathbf{x})} d\pi(\mathbf{x}) = P_t \frac{\rho_0}{\pi}(\tilde{\mathbf{x}}) \quad (7)$$

The above derivation yields two equivalent characterisations of the exact solution of the forward process in terms of the density ratio ρ_t/π :

Characterization as a time-dependent kernel mean embedding There is a rich literature on the embedding of probability distributions into Hilbert spaces (Smola et al., 2007; Gretton et al., 2012; Muandet et al., 2017). Recall that a symmetric semi-positive definite function $k : \mathbb{R}^d \times \mathbb{R}^d \rightarrow \mathbb{R}$ is called a *kernel*, and is uniquely associated with a reproducing kernel Hilbert space (RKHS) denoted $\mathcal{H}(k)$. Any distribution ν on \mathbb{R}^d for which $\mathbf{x} \mapsto \sqrt{k(\mathbf{x}, \mathbf{x})}$ is ν -integrable can be *embedded* into $\mathcal{H}(k)$ according to

$$\nu \mapsto \mu_\nu, \quad \mu_\nu(\tilde{\mathbf{x}}) := \int k(\mathbf{x}, \tilde{\mathbf{x}}) d\nu(\mathbf{x}),$$

called the KME. The KME enables the mathematical structure of the RKHS to be brought to bear on the set of probability distributions¹. Thus (7) reveals that the density ratio ρ_t/π is the image under the k_t -KME of the data-generating distribution:

$$\mu_{\rho_0}^{(t)}(\tilde{\mathbf{x}}) := \frac{\rho_t}{\pi}(\tilde{\mathbf{x}}) = \int k_t(\mathbf{x}, \tilde{\mathbf{x}}) d\rho_0(\mathbf{x}) \quad (8)$$

That is, for each $t > 0$ we have a kernel k_t such that ρ_t/π is an element of $\mathcal{H}(k_t)$. For the Mehler kernel (6), $\mathcal{H}(k_t)$ interpolates between $L^2(\pi)$ (as $t \rightarrow 0$) and a space of constant functions (as $t \rightarrow \infty$), indicating that ρ_t/π becomes more regular as t is increased.

An apparently natural idea is to approximate (8) by plugging in the empirical distribution $\hat{\rho}_0$ of the dataset, ameliorating the need for neural score matching to train a DM. Much is known about the statistical and computational aspects of approximating a KME based on samples, and these existing results can in principle be directly applied (e.g. Sriperumbudur et al., 2011; Tolstikhin et al., 2017). Some specific consequences of the connection we have unveiled here between kernel embedding of distributions and DMs are discussed in Section 3.

Characterization as the action of the Markov semigroup operator The second characterisation we obtained in (7) reveals that the density ratio ρ_t/π is given by the action of the Markov semigroup operator P_t on the ratio ρ_0/π of the data-generating distribution ρ_0 and the stationary distribution π . This characterization in particular reveals the appeal of a *Markov* diffusion process, as well as representing ρ_t using density ratio ρ_t/π , as opposed to the Lebesgue density ρ_t itself. Indeed, while the conventional neural approximations used in score-matching view the score function $\nabla \log \rho_t(\mathbf{x})$ as a generic time-dependent vector field, the t dependence of $(\rho_t/\pi)(\mathbf{x})$ becomes *disentangled* from the \mathbf{x} dependence when we interpret this ratio as the action of P_t on the ratio ρ_0/π . This in turn enables a streamlined derivation of score matching and related objectives, as shown next in Section 2.3.

¹For example, the difference between a pair of distributions ν and η can be measured using the maximum mean discrepancy (MMD) $D_k(\nu, \eta)^2 := \langle \mu_\nu, \mu_\nu \rangle - 2\langle \mu_\nu, \mu_\eta \rangle + \langle \mu_\eta, \mu_\eta \rangle$ (Gretton et al., 2012).

2.3 Score Matching via the Carré-du-Champ and Dirichlet Operators

Accurate approximation of the score function $\nabla \log \rho_t(\mathbf{x})$ is critical to the success of DM. The standard approach is based on score matching (Hyvärinen, 2005), wherein a time-dependent vector field $\mathbf{s}_t(\mathbf{x})$ is trained to minimize an L^2 distance to the true score function $\mathbf{s}_t^*(\mathbf{x})$:

$$\min_{\mathbf{s}} \int_{t=0}^T \mathbb{E}_{\mathbf{X}_t \sim \rho_t} \|\mathbf{s}_t(\mathbf{X}_t) - \mathbf{s}_t^*(\mathbf{X}_t)\|^2 w(t) dt, \quad \mathbf{s}_t^*(\mathbf{x}) := \nabla \log \frac{\rho_t}{\pi}(\mathbf{x}) \quad (9)$$

for some non-negative weight function $w(t)$ that must be specified. Integration by parts is required to circumvent the fact that $\nabla \log \rho_t$ is intractable in general. The Markov diffusion operator perspective enables a streamlined derivation of the standard score matching objective, as well as a new insight into related objectives, as will now be demonstrated.

Markov diffusion operators naturally give rise to a (generalized) integration by parts formula for integrals with respect to the stationary measure π of the DM. To this end, we introduce the *carré-du-champ* operator $\Gamma(\cdot, \cdot)$ and the *Dirichlet* operator $\mathcal{E}(\cdot, \cdot)$, defined as

$$\Gamma(f, g) := \frac{1}{2} (\mathcal{L}(fg) - f\mathcal{L}g - g\mathcal{L}f), \quad \mathcal{E}(f, g) = \int \Gamma(f(\mathbf{x}), g(\mathbf{x})) d\pi(\mathbf{x});$$

see Bakry et al. (2013) for background. The integration by parts formula is then expressed as the self-adjointness of \mathcal{L} when integrating over π ; namely,

$$\int \Gamma(f, g) d\pi = \mathcal{E}(f, g) = - \int f\mathcal{L}g d\pi = - \int g\mathcal{L}f d\pi. \quad (10)$$

The symmetry of the Mehler kernel implies the self-adjointness of \mathcal{L} , see Bakry et al. (Chap. 1 2013). The standard integration by parts formula is recovered as the (degenerate) case corresponding to the BM process, whose stationary measure is nominally the Lebesgue measure dx .

Example 4 (OU process, continued) For the OU process the carré-du-champ operator is $\Gamma(f, g) = \langle \nabla f, \nabla g \rangle$ and the Dirichlet operator is the L^2 inner product $\mathcal{E}(f, g) = \int \langle \nabla f(\mathbf{x}), \nabla g(\mathbf{x}) \rangle d\pi(\mathbf{x})$.

Streamlined derivation of score matching Letting $\mathbf{s}_t(\mathbf{x}) = \nabla f_t(\mathbf{x})$, score-matching aims to minimise an L^2 loss between the score function and its approximation:

$$\begin{aligned} \mathcal{L}(f_t) &:= \mathbb{E}_{\mathbf{X}_t \sim \rho_t} \left\| \nabla f_t(\mathbf{X}_t) - \nabla \log \frac{\rho_t}{\pi}(\mathbf{X}_t) \right\|^2 \\ &\stackrel{+C}{=} \mathbb{E}_{\mathbf{X}_t \sim \rho_t} \left[\|\nabla f_t(\mathbf{X}_t)\|^2 - 2 \left\langle \nabla f_t(\mathbf{X}_t), \nabla \log \frac{\rho_t}{\pi}(\mathbf{X}_t) \right\rangle \right] \end{aligned} \quad (11)$$

where we have used $\stackrel{+C}{=}$ to indicate equality up to an f_t -independent additive constant. The final term in (11) can be simplified using (generalized) integration by parts (10), to obtain the equivalent expression

$$\begin{aligned} \int \left\langle \nabla f_t(\mathbf{x}), \nabla \log \frac{\rho_t}{\pi}(\mathbf{x}) \right\rangle d\rho_t(\mathbf{x}) &= \int \left\langle \nabla f_t(\mathbf{x}), \nabla \frac{\rho_t}{\pi}(\mathbf{x}) \right\rangle d\pi(\mathbf{x}) \\ &= \mathcal{E}\left(f_t, \frac{\rho_t}{\pi}\right) = - \int \mathcal{L}f_t(\mathbf{x}) \frac{\rho_t}{\pi}(\mathbf{x}) d\pi(\mathbf{x}) = -\mathbb{E}_{\mathbf{X}_t \sim \rho_t} \mathcal{L}f_t(\mathbf{X}_t). \end{aligned}$$

Substituting back into (11) we obtain

$$\mathcal{L}(f_t) \stackrel{+C}{=} \mathbb{E}_{\mathbf{X}_t \sim \rho_t} \left[\|\nabla f_t(\mathbf{X}_0)\|^2 + 2\mathcal{L}f_t(\mathbf{X}_0) \right], \quad (12)$$

which recovers the practical score matching objective of Hyvärinen (2005), generalized to any infinitesimal generator \mathcal{L} , and requiring only regularity on ρ_t/π , instead of on the *individual* densities of ρ_t and π . As an additional bonus of the Markov diffusion operator perspective, we can exploit the symmetry of P_t to shift the expectation with respect to the data distribution, so that

$$\mathcal{L}(f_t) \stackrel{+C}{=} \mathbb{E}_{\mathbf{X}_0 \sim \rho_0} P_t \left[\|\nabla f_t(\mathbf{X}_0)\|^2 + 2\mathcal{L}f_t(\mathbf{X}_0) \right], \quad (13)$$

which follows since $\mathbb{E}_{\mathbf{X}_t \sim \rho_t} g(\mathbf{X}_t) = \int g(\mathbf{x}) P_t \frac{\rho_0}{\pi}(\mathbf{x}) d\pi(\mathbf{x}) = \mathbb{E}_{\mathbf{X}_0 \sim \rho_0} P_t g(\mathbf{X}_0)$. This observation underpins our proposed *operator-informed score matching* methodology in Section 4. Through the lens of Markov diffusion operators we also gain new insight into *Tweedie's formula* (Tweedie, 1947), *time score matching* (Choi et al., 2022), and a generalization of the *score Fokker–Planck equation* (FPE) (Lai et al., 2023a); these are presented in Appendix B.

3 Insight from Exact Solution of the Forward Process

The explicit solution to the forward process obtained in Section 2.2 established an equivalence between kernel density estimation and DM, as plugging in the empirical distribution $\hat{\rho}_0$ of the dataset gives a consistent estimator of the KME

$$\mu_{\hat{\rho}_0}^{(t)}(\mathbf{x}) = \frac{1}{N} \sum_{n=1}^N k_t(\mathbf{x}, \mathbf{x}_n) \rightarrow \mu_{\rho_0}^{(t)}(\mathbf{x}) \quad \text{as } N \rightarrow \infty. \quad (14)$$

This estimator is widely used in machine learning, but suffers from two major drawbacks in the context of DM. First, one simply obtains samples from the original dataset when simulating the backward process with (14); no generalization has occurred. Secondly, the empirical embedding suffers from the *Stein effect* (Muandet et al., 2014), a pathology analogous to the suboptimality of the empirical mean estimator for multivariate Gaussian distributions (Stein, 1956). Motivated by these observations, we next consider the use of alternative shrinkage estimators, showing how this leads to an improved approach to estimation of the KME in the DM context.

Diffusion kernel smoothing Given a reference measure π and a set of orthonormal basis function $(\varphi_n)_{n \geq 0}$ spanning $L^2(\pi)$, we can express the density ratio in this coordinate system:

$$\frac{\rho_0}{\pi}(\tilde{\mathbf{x}}) = \sum_{n=0}^{\infty} \alpha_n \varphi_n(\tilde{\mathbf{x}}), \quad \alpha_n := \mathbb{E}_{\mathbf{x} \sim \rho_0}[\varphi_n(\mathbf{x})] \quad (15)$$

As each α_n can be represented as an expectation w.r.t. ρ_0 , (15) suggests a potential estimator for ρ_0/π , where each coefficient is evaluated by the empirical measure: $\hat{\alpha}_n = \mathbb{E}_{\mathbf{x} \sim \hat{\rho}_0}[\varphi_n(\mathbf{x})]$. However, the performance of the empirical mean is gated by the Stein effect². Much research has been devoted to smoothing the coefficients with shrinkage estimators, and we discuss related work in Appendix C.

Specialising the φ_n to be the eigenfunctions ϕ_n of the generator \mathcal{L} (corresponding to eigenvalues λ_n ; c.f. Section 2.1), Botev et al. (2010, Remark 3) introduced the diffusion kernel smoother (DKS)³, which is controlled by a bandwidth $s > 0$ and based on (4):

$$\frac{\check{\rho}_0}{\pi}(\tilde{\mathbf{x}}) := \mu_{\check{\rho}_0}^{(s)}(\tilde{\mathbf{x}}) = \int k_s(\mathbf{x}, \tilde{\mathbf{x}}) d\hat{\rho}_0(\mathbf{x}) = \sum_{n=0}^{\infty} e^{\lambda_n s} \hat{\alpha}_n \phi_n(\tilde{\mathbf{x}}) \quad (16)$$

Despite the drawbacks of high-dimensional kernel density estimators in general, we highlight that the DKS (16) induces an estimator for all noise-perturbed distributions *simultaneously*, and may therefore be well-suited to DM. Indeed, we obtain closed-form estimators for all ρ_t/π whose $L^2(\pi)$ error is *uniformly bounded* by the error of the initial estimate in (16):

$$\frac{\check{\rho}_t}{\pi}(\mathbf{x}) := P_t \frac{\check{\rho}_0}{\pi}(\mathbf{x}) = \mu_{\check{\rho}_0}^{(s+t)}(\mathbf{x}), \quad \left\| \frac{\check{\rho}_t}{\pi} - \frac{\rho_t}{\pi} \right\|_{L^2(\pi)} \leq e^{-t} \left\| \frac{\check{\rho}_0}{\pi} - \frac{\rho_0}{\pi} \right\|_{L^2(\pi)} \quad (17)$$

The exponentially decaying rate of error is a consequence of the Poincaré inequalities associated with the diffusion operators: see Theorem 4.2.5 of Bakry et al. (2013). Further, the estimators $\check{\rho}_t/\pi$ automatically satisfy regularity constraints, as $\check{\rho}_t/\pi$ resides in the same Hilbert space $\mathcal{H}(k_t)$ as the ground truth ρ_t/π ; a consequence of the inclusion $\mathcal{H}(k_{t+s}) \subset \mathcal{H}(k_t)$. Motivated by this example, we propose a more flexible kernel smoothing that remains closed-form under P_t .

Riemannian diffusion kernel smoothing The DKS in (16) performs uniform smoothing across all dimensions, limiting its potential to uncover the data manifold. As a solution, we propose to combine a more flexible *Riemannian Langevin diffusion* (Girolami and Calderhead, 2011) with DKS, while preserving the same standard Gaussian target:

$$d\mathbf{X}_t = [-\mathbf{\Lambda}(\mathbf{X}_t)\mathbf{X}_t + \langle \nabla, \mathbf{\Lambda}(\mathbf{X}_t) \rangle] dt + \sqrt{2\mathbf{\Lambda}(\mathbf{X}_t)} d\mathbf{W}_t, \quad (18)$$

where $\mathbf{\Lambda}(\cdot)$ is a positive definite matrix-valued function representing the *metric tensor*, a degree of freedom whose estimation, it is shown below, can enable more effective characterization of the data manifold. Though the associated kernel k_s no longer has a closed-form in general, for small s it can be accurately approximated

$$k_{s;\mathbf{\Lambda}}(\tilde{\mathbf{x}}, \mathbf{x}) \approx \det(\mathbf{I} - \mathbf{P}_s)^{-1/2} \exp\left(-\frac{\mathbf{x}^\top \mathbf{A}_s \mathbf{x} + \tilde{\mathbf{x}}^\top \mathbf{A}_s \tilde{\mathbf{x}} - 2\mathbf{x}^\top \mathbf{B}_s \tilde{\mathbf{x}}}{2}\right), \quad (19)$$

where $\mathbf{P}_s := e^{-s\mathbf{\Lambda}(\mathbf{x})}$, $\mathbf{B}_s := (\mathbf{I} - \mathbf{P}_s)^{-1} \mathbf{P}_s$, $\mathbf{A}_s := \mathbf{P}_s \mathbf{B}_s$. This approximation is obtained by treating the metric tensor as locally constant; full justification is provided in Appendix A.4.

²Chapter 8 of Wasserman (2005) suggests an equivalence between estimating the α_n coefficients and estimating the mean of a multivariate Gaussian, thus justifying the use of James–Stein shrinkage estimators in this context.

³Our terminology.

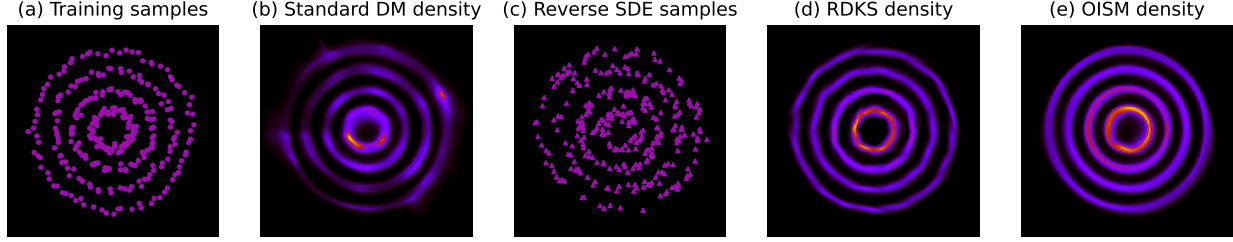


Figure 1: An empirical proof-of-concept. The task is to construct a generative model for p_{data} based on the training dataset consisting of independent samples from p_{data} in (a). Standard diffusing modelling (DM) produced the density estimate in (b), and the samples in (c) were generated from this DM using the SDE-based stochastic sampler of Song and Ermon (2020). Our proposed *Riemannian diffusion kernel smoothing* (RDKS) and *operator-informed score matching* (OISM) methods are presented respectively in (d) and (e). Computational costs were equal for (b) and (e). Additional experiments are reported in Appendix D.3.

Illustrative experiment Since this paper’s primary focus is on theory, the experiment that we present next is limited to a proof-of-concept. To this end, we considered a two-dimensional task and implemented Riemannian DKS (RDKS) by treating the metric tensor as a collection of hyperparameters $\Lambda(\mathbf{x}_n) = \Lambda_n$ defined at each point in the dataset. As we can express $\mathcal{L} \log \check{\rho}_t / \pi$ in terms of the hyperparameters Λ_n , the score matching objective of (12) can be optimized with respect to the Λ_n . Results from our proposed RDKS generative model are displayed in Figure 1, where they are contrasted to standard DM. The density learned using standard DM does not accurately capture the data manifold in this task, though somewhat realistic samples can still be generated via injection of additional noise using the SDE-based stochastic sampler of Song and Ermon (2020). In contrast, the density learned using RDKS (and hence also samples generated by reversing the probability flow ODE) more accurately capture the data manifold. Full experimental details can be found in Appendix D.

This proof-of-concept suggests the importance of noise perturbation for detecting the data manifold, and that RDKS can ameliorate the burden of neural score estimation by exact solution of the forward process in a Markov DM, at least in a low-dimensional context. In contrast to standard DM, which starts with zero knowledge of the score function and optimizes towards the perfectly memorized dataset (as noted in Corollary 1 of Pidstrigach, 2022), RDKS starts from the optimal yet undesirable memorized scores and then tries to explore the data manifold. Both approaches involve implicit regularization; neural network inductive bias in standard DM, and the implicit parameter shrinkage in RDKS. Further work will be required to understand how the implicit biases of RDKS compare with those of standard DM.

4 Operator-Informed Score Matching

Finally, building on our theoretical insights up to this point, we present a novel variance reduction technique called operator-informed score matching (OISM), that is straightforward to implement within existing frameworks for DM.

Linear score approximator To motivate a low-order approximation to the score function, we observe from Example 3 that low-order polynomials are eigenfunctions of the OU infinitesimal generator \mathcal{L} . For instance, with arbitrary matrix \mathbf{U} and vector \mathbf{v} , $\mathbf{x}^\top \mathbf{U} \mathbf{x} - \text{tr}(\mathbf{U})$ has eigenvalue 2; $\mathbf{v}^\top \mathbf{x}$ has eigenvalue 1. From (13), we can *exactly* solve for an optimal linear score matching estimator of the form $\hat{\mathbf{s}}_t^*(\mathbf{x}) \approx \mathbf{s}_t(\mathbf{x}) := \nabla f_t(\mathbf{x})$ with $f_t(\mathbf{x}) = -\frac{1}{2} \mathbf{x}^\top \mathbf{A}_t \mathbf{x} + \mathbf{b}_t^\top \mathbf{x}$ for all $t > 0$, *without* requiring the forward process to be simulated:

$$\begin{aligned} (\mathbf{A}_t, \mathbf{b}_t) &= \arg \min_{\mathbf{A}, \mathbf{b}} \mathbb{E}_{\mathbf{x} \sim \hat{\rho}_0} P_t \left[\|\mathbf{A} \mathbf{x} + \mathbf{b}\|^2 + 2[-\text{tr}(\mathbf{A}) - \mathbf{x}^\top (-\mathbf{A} \mathbf{x} + \mathbf{b})] \right] \\ &= \arg \min_{\mathbf{A}, \mathbf{b}} \mathbb{E}_{\mathbf{x} \sim \hat{\rho}_0} \left[\begin{aligned} &\alpha_t^2 \langle \mathbf{A} \mathbf{A}^\top, \mathbf{x} \mathbf{x}^\top \rangle_F + 2\alpha_t^2 \langle \mathbf{A}^\top, \mathbf{x} \mathbf{x}^\top \rangle_F - 2\alpha_t \mathbf{b}^\top (\mathbf{A} \mathbf{x} + \mathbf{x}) \\ &+ \sigma_t^2 \|\mathbf{A}\|_F^2 + \|\mathbf{b}\|^2 - 2\alpha_t^2 \text{tr}(\mathbf{A}) \end{aligned} \right], \end{aligned}$$

where the F subscript denotes the Frobenius norm or inner product. The above quadratic optimization can be exactly solved, leading to the linear approximation

$$\hat{\mathbf{s}}_t(\mathbf{x}) = (\mathbf{I} - (\alpha_t^2 \hat{\Sigma} + \sigma_t^2 \mathbf{I})^{-1}) \mathbf{x} + \alpha_t (\alpha_t^2 \hat{\Sigma} + \sigma_t^2 \mathbf{I})^{-1} \hat{\boldsymbol{\mu}}, \quad (20)$$

involving the empirical mean $\hat{\boldsymbol{\mu}}$ and covariance $\hat{\Sigma}$ of the dataset. Though a linear score estimator is clearly insufficient to describe complex densities, it provides a useful variance reduction tool: Specifically, we can construct an *operator-informed* score estimator of the form $\hat{\mathbf{s}}_t(\mathbf{x}) + \mathbf{r}_t(\mathbf{x})$, where $\hat{\mathbf{s}}_t(\mathbf{x})$ provides a closed-form approximation and a neural

network $\mathbf{r}_t(\mathbf{x})$ is fit to the residual. Being operator-based, this approach is applicable to other Markov DMs for which diffusion operators can be computed; see Appendix A.

Higher-order score approximators for the OU process Higher-order approximations to the score function can be constructed using general combinations of eigenfunctions: $f_t(\mathbf{x}) = \sum_{i \in \mathcal{I}} \beta_i(t) \phi_i(\mathbf{x})$, where for the OU process the ϕ_i are Hermite polynomials (c.f. Example 3). Then, again following from (13), the score-matching estimator can be characterized as the solution to

$$\min_{\beta} \mathbb{E}_{\mathbf{x} \sim \hat{\rho}_0} \left[\underbrace{\sum_{j \in \mathcal{J}} e^{\lambda_j t} \gamma_{j;\beta(t)} \phi_j(\mathbf{x})}_{=P_t \|\nabla f_t\|^2} + 2 \underbrace{\sum_{i \in \mathcal{I}} e^{\lambda_i t} \lambda_i \beta_i(t) \phi_i(\mathbf{x})}_{=P_t \mathcal{L} f_t} \right], \quad (21)$$

where the coefficients $\gamma_{j;\beta(t)}$ arise from converting products $\phi_i \phi_j$, which appear in calculation of the term $P_t \|\nabla f_t\|^2$, into linear combinations of the ϕ_i on an extended eigenfunction set \mathcal{J} . This is possible for the OU process since the ϕ_i are polynomial, and the product of two polynomials is again polynomial. The coefficients $\gamma_{j;\beta(t)}$ can be obtained as the solution of a linear system of equations; see Appendix A.5.

Illustrative experiment The performance of OISM is also illustrated in Figure 1, where it is seen to outperform both standard DM and RDKS. Full experimental details can be found in Appendix D. In addition, we showcase in Appendix E that in a higher-dimensional setting, learning the residual scores alongside a linear score estimator yields similar results while providing marginal improvements on the deterministic simulation of samples using the probability flow ODE (3). The SDE-based stochastic sampler of Song and Ermon (2020) can be seen as the sum of (3) and a Langevin diffusion converging to ρ_t at each time t ; linear OISM achieves the same effect by enforcing convergence towards a Gaussian approximation of ρ_t . Higher-order score approximations has the potential to give better-informed closed-form score estimates, but further investigation in practical settings is required.

5 Discussion

This paper contributes to an improved theoretical understanding of DM, establishing connections to diffusion operators, kernel embeddings, and density ratio estimation; as a by-product, the novel RDKS and OISM methods were also proposed. In the remainder we discuss related work and the limitations and potential of the methods we have proposed.

Related Work Here we highlight two recent papers that discussed the interplay between the forward process and score matching in detail. First, Scarvelis et al. (2023) considered a simple forward process taking the form of a weighted mixture of the data distribution p_{data} and the noise distribution π , so that both the forward process and the associated scores can be exactly computed. This approach circumvents neural approximation of score functions, but introduces a performance gap relative to the state-of-the-art for tasks such as image generation. Our contribution differed in that we focused on standard Markov DMs and investigated in detail theoretical aspects of memorization and smoothing, developing a systematic methodology for smoothing in the DM context. Second, Lai et al. (2023a) considered a Markov DM and observed that the score functions associated to the noise-perturbed distributions satisfy a FPE. The authors then developed a regularized version of score-matching in which the score FPE is approximately enforced; we showed in Appendix B that score FPE can be expressed in terms of Markov diffusion operators, providing additional insight into this method. Our approach differed to this work in that we further leveraged the spectral properties of Markov diffusion operators to obtain novel score estimators that *automatically* conform to the constraints of a Markov DM.

Limitations and Potential This work presented a novel viewpoint of encoding diffusion operators into score-based generative modeling; however, our investigation was mostly theoretical and our illustrations were limited to proofs-of-concept. The proposed RDKS method can in principle circumvent neural score approximation in Markov DMs, but relies on estimation of the metric tensor, i.e. the data manifold. Further work will be required to investigate whether Riemannian DKS can be made to work in a high-dimensional context. The linear version of OISM is immediately applicable and demonstrated practical potential, but further work (e.g. tensorization of Hermite polynomials) will be needed to make higher-order approximation of the score function practical.

Despite these limitations, our contribution supports the view that Markov diffusion operators provide valuable insight into DM, and have the potential both to improve existing methods and inspire new methodological development.

Acknowledgments and Disclosure of Funding

ZS and CJO were supported by EP/W019590/1.

References

- Bakry, D., Gentil, I., and Ledoux, M. *Analysis and Geometry of Markov Diffusion Operators*. Springer, New York, 2013. ISBN 978-3-319-00226-2.
- Bansal, A., Borgnia, E., Chu, H.M., Li, J.S., Kazemi, H., Huang, F., Goldblum, M., Geiping, J., and Goldstein, T. Cold Diffusion: Inverting Arbitrary Image Transforms Without Noise. In *Proceedings of the 37th Conference on Neural Information Processing Systems*, 2023.
- Beran, R. REACT Scatterplot Smoothers: Superefficiency through Basis Economy. *Journal of the American Statistical Association*, 95(449):155–171, 2000.
- Beran, R. and Dumbgen, L. Modulation of Estimators and Confidence Sets. *The Annals of Statistics*, 26(5):1826–1856, 1998.
- Botev, Z.I., Grotowski, J.F., and Kroese, D.P. Kernel density estimation via diffusion. *The Annals of Statistics*, 38(5), 2010.
- Choi, K., Meng, C., Song, Y., and Ermon, S. Density Ratio Estimation via Infinitesimal Classification. In *Proceedings of The 25th International Conference on Artificial Intelligence and Statistics*, pages 2552–2573. PMLR, 2022.
- Corso, G., Jing, B., Barzilay, R., Jaakkola, T., et al. DiffDock: Diffusion steps, twists, and turns for molecular docking. In *Proceedings of the 11th International Conference on Learning Representations*, 2023.
- Dockhorn, T., Vahdat, A., and Kreis, K. Score-Based Generative Modeling with Critically-Damped Langevin Diffusion. In *Proceedings of the 9th International Conference on Learning Representations*, 2021.
- Efromovich, S. *Nonparametric Curve Estimation: Methods, Theory, and Applications*. Springer, 2013. ISBN 978-1-4757-7301-9.
- Efron, B. Tweedie’s Formula and Selection Bias. *Journal of the American Statistical Association*, 106(496):1602–1614, 2011.
- Girolami, M. and Calderhead, B. Riemann manifold Langevin and Hamiltonian Monte Carlo methods. *Journal of the Royal Statistical Society: Series B (Statistical Methodology)*, 73(2):123–214, 2011.
- Glad, I.K., Hjort, N.L., and Ushakov, N.G. Correction of Density Estimators That Are Not Densities. *Scandinavian Journal of Statistics*, 30(2):415–427, 2003.
- Gretton, A., Borgwardt, K.M., Rasch, M.J., Schölkopf, B., and Smola, A. A Kernel Two-Sample Test. *Journal of Machine Learning Research*, 13(25):723–773, 2012.
- Ho, J., Jain, A., and Abbeel, P. Denoising diffusion probabilistic models. In *Proceedings of the 34th Conference on Neural Information Processing Systems*, pages 6840–6851, 2020.
- Hyvärinen, A. Estimation of Non-Normalized Statistical Models by Score Matching. *Journal of Machine Learning Research*, 6(24):695–709, 2005.
- Lai, C.H., Takida, Y., Murata, N., Uesaka, T., Mitsufuji, Y., and Ermon, S. FP-Diffusion: Improving Score-based Diffusion Models by Enforcing the Underlying Score Fokker-Planck Equation. In *Proceedings of the 40th International Conference on Machine Learning*, 2023a.
- Lai, C.H., Takida, Y., Murata, N., Uesaka, T., Mitsufuji, Y., and Ermon, S. FP-Diffusion: Improving score-based diffusion models by enforcing the underlying score Fokker-Planck equation. In *Proceedings of the 40th International Conference on Machine Learning*, 2023b.
- Mehler, F. Ueber die Entwicklung einer Function von beliebig vielen Variablen nach Laplaceschen Functionen höherer Ordnung. *Journal für die Reine und Angewandte Mathematik*, 66:161–176, 1866.
- Muandet, K., Fukumizu, K., Sriperumbudur, B., Gretton, A., and Schoelkopf, B. Kernel Mean Estimation and Stein Effect. In *Proceedings of the 31st International Conference on Machine Learning*, pages 10–18, 2014.
- Muandet, K., Fukumizu, K., Sriperumbudur, B., Schölkopf, B., et al. Kernel mean embedding of distributions: A review and beyond. *Foundations and Trends® in Machine Learning*, 10(1-2):1–141, 2017.
- Øksendal, B. *Stochastic Differential Equations: An Introduction with Applications*. Springer, Berlin Heidelberg New York Dordrecht London, 6th ed. 2003 edition edition, 2003. ISBN 978-3-540-04758-2.
- Pidstrigach, J. Score-Based Generative Models Detect Manifolds. In *Proceedings of the 36th Conference on Neural Information Processing Systems*, volume 35, 2022.
- Poole, B., Jain, A., Barron, J.T., and Mildenhall, B. DreamFusion: Text-to-3D using 2D Diffusion. In *Proceedings of the 11th International Conference on Learning Representations*, 2022.

- Rhodes, B., Xu, K., and Gutmann, M.U. Telescoping Density-Ratio Estimation. In *Proceedings of the 34th Conference on Neural Information Processing Systems*, 2020.
- Robbins, H. An Empirical Bayes Approach to Statistics. In *Proceedings of the Third Berkeley Symposium on Mathematical Statistics and Probability, Volume 1: Contributions to the Theory of Statistics*, pages 157–164. University of California Press, 1956.
- Rombach, R., Blattmann, A., Lorenz, D., Esser, P., and Ommer, B. High-resolution image synthesis with latent diffusion models. In *Proceedings of the IEEE/CVF Conference on Computer Vision and Pattern Recognition*, pages 10684–10695, 2022.
- Särkkä, S. and Solin, A. *Applied Stochastic Differential Equations*. Cambridge University Press, 2019. ISBN 978-1-316-64946-6.
- Scarvelis, C., Borde, H.S.d.O., and Solomon, J. Closed-Form Diffusion Models. *arXiv:2310.12395*, 2023.
- Smola, A., Gretton, A., Song, L., and Schölkopf, B. A Hilbert Space Embedding for Distributions. In Hutter, M., Servedio, R.A., and Takimoto, E., editors, *Algorithmic Learning Theory*, Lecture Notes in Computer Science, pages 13–31. Springer, 2007. ISBN 978-3-540-75225-7.
- Sohl-Dickstein, J., Weiss, E., Maheswaranathan, N., and Ganguli, S. Deep unsupervised learning using nonequilibrium thermodynamics. In *Proceedings of the 32nd International Conference on Machine Learning*, 2015.
- Song, Y. and Ermon, S. Generative Modeling by Estimating Gradients of the Data Distribution. In *Proceedings of the 33rd Conference on Neural Information Processing Systems*, 2019.
- Song, Y. and Ermon, S. Improved Techniques for Training Score-Based Generative Models. In *Advances in Neural Information Processing Systems*, volume 33, pages 12438–12448. Curran Associates, Inc., 2020.
- Song, Y., Sohl-Dickstein, J., Kingma, D.P., Kumar, A., Ermon, S., and Poole, B. Score-Based Generative Modeling through Stochastic Differential Equations. In *Proceedings of the 8th International Conference on Learning Representations*, 2020.
- Sriperumbudur, B.K., Fukumizu, K., and Lanckriet, G.R. Universality, characteristic kernels and RKHS embedding of measures. *Journal of Machine Learning Research*, 12(7), 2011.
- Stein, C. Inadmissibility of the Usual Estimator for the Mean of a Multivariate Normal Distribution. In *Proceedings of the Third Berkeley Symposium on Mathematical Statistics and Probability, Volume 1: Contributions to the Theory of Statistics*, pages 197–207. University of California Press, 1956.
- Stroock, D.W. *An Introduction to Markov Processes*. Springer Science & Business Media, 2013.
- Sugiyama, M., Suzuki, T., and Kanamori, T. *Density Ratio Estimation in Machine Learning*. Cambridge University Press, New York, 2012. ISBN 978-0-521-19017-6.
- Tolstikhin, I., Sriperumbudur, B.K., and Mu, K. Minimax estimation of kernel mean embeddings. *Journal of Machine Learning Research*, 18(86):1–47, 2017.
- Tweedie, M.C.K. Functions of a statistical variate with given means, with special reference to Laplacian distributions. *Mathematical Proceedings of the Cambridge Philosophical Society*, 43(1):41–49, 1947. ISSN 1469-8064, 0305-0041.
- Vincent, P. A Connection Between Score Matching and Denoising Autoencoders. *Neural Computation*, 23(7): 1661–1674, 2011.
- Wasserman, L. *All of Nonparametric Statistics*. Springer, New York, 2005. ISBN 978-0-387-25145-5.
- Watson, G.S. Density Estimation by Orthogonal Series. *The Annals of Mathematical Statistics*, 40(4):1496–1498, 1969.
- Whittle, P. On the Smoothing of Probability Density Functions. *Journal of the Royal Statistical Society. Series B (Methodological)*, 20(2):334–343, 1958.

Appendices

Appendix A presents the Markov diffusion operators for a more general class of LTI SDEs. Appendix B explores further consequences of Markov diffusion operators in the context of related work, including Tweedie’s formula (Tweedie, 1947), time score matching (Choi et al., 2022), and the score FPE (Lai et al., 2023b). Related work on the use of orthogonal series for density estimation is reviewed in Appendix C. Full details required to reproduce our two-dimensional experiment are contained in Appendix D, and full details to reproduce the MNIST experiment are contained in Appendix E.

A Diffusion Operators for Markov Forward Processes

This appendix presents Markov diffusion operators for a wider class of LTI SDEs, generalizing beyond the OU process featured in the main text. Chapter 6 of Särkkä and Solin (2019) contains helpful explanations on this topic. LTI SDEs take the form of the following Itô diffusion:

$$d\mathbf{X}_t = \mathbf{F}\mathbf{X}_t + \mathbf{L} d\mathbf{W}_t \quad (22)$$

The above formula covers most diffusion forward processes, namely, BM with $\mathbf{F} = \mathbf{0}, \mathbf{L} = \sqrt{2}\mathbf{I}$, OU with $\mathbf{F} = -\mathbf{I}, \mathbf{L} = \sqrt{2}\mathbf{I}$, as well as recent efforts of dampening the forward processes with momentum variables, with

$$\mathbf{F} = \begin{pmatrix} \mathbf{0} & \mathbf{I} \\ -\mathbf{I} & -c\mathbf{I} \end{pmatrix}, \quad \mathbf{L} = \begin{pmatrix} \mathbf{0} & \mathbf{0} \\ \mathbf{0} & \sqrt{2c}\mathbf{I} \end{pmatrix};$$

see Dockhorn et al. (2021). The stationary measure and Markov semigroup associated with (22) are discussed in Appendix A.1. The infinitesimal generator and carré-du-champ operators are discussed in Appendix A.2, and the spectrum of the infinitesimal generator is discussed in Appendix A.3. The case of a Riemannian Langevin diffusion is discussed in Appendix A.4. Lastly, some useful properties of Hermite polynomials (the eigenfunctions of the infinitesimal generator of the OU process) are contained in Appendix A.5.

A.1 Characterizing the Stationary Measure and Markov Semigroup

The existence of a stationary probability measure π for (22) is determined by the eigenvalues of \mathbf{F} : If the real parts of the eigenvalues of \mathbf{F} are strictly negative, (22) evolves towards a zero-mean Gaussian distribution $\mathcal{N}(\mathbf{0}, \Sigma_\infty)$. The covariance matrix Σ_∞ satisfies the following Lyapunov equation (eq. 6.69 of Särkkä and Solin (2019)):

$$\mathbf{F}\Sigma_\infty + \Sigma_\infty\mathbf{F}^\top + \mathbf{L}\mathbf{L}^\top = \mathbf{0}$$

The intermediate distributions of (22) has the following closed form solution:

$$\rho_t(\tilde{\mathbf{x}}|\mathbf{x}) = \mathcal{N}(\tilde{\mathbf{x}}|\mathbf{A}_t\mathbf{x}, \Sigma_t), \quad \mathbf{A}_t = \exp(t\mathbf{F}), \quad \Sigma_t = \Sigma_\infty - \mathbf{A}_t\Sigma_\infty\mathbf{A}_t^\top$$

Therefore, the symmetrized Markov density kernel takes the following form:

$$k_t(\tilde{\mathbf{x}}, \mathbf{x}) = \frac{\rho_t(\tilde{\mathbf{x}}|\mathbf{x})}{\mathcal{N}(\tilde{\mathbf{x}}|\mathbf{0}, \Sigma_\infty)} \quad (23)$$

The BM process (c.f. Example 1) requires some special treatment as we nominally refer to the Lebesgue measure as the target measure π , yielding a Markov density kernel

$$k_t(\tilde{\mathbf{x}}, \mathbf{x}) = (2\pi t)^{-d/2} \exp\left(-\frac{\|\tilde{\mathbf{x}} - \mathbf{x}\|^2}{2t}\right). \quad (24)$$

The formula (23) and (24) naturally define the specific form of the Markov semigroup $(P_t)_{t \geq 0}$, as well as the symmetrized Markov density kernel for mean embedding.

A.2 Infinitesimal Generators and Carré-du-Champ Operators

Here we characterise the infinitesimal generators and carré-du-champ operators for SDEs of the form (22), based on relevant results from Sections 1.10 and 1.11 of Bakry et al. (2013). Denoting $\mathbf{G} = \frac{1}{2}\mathbf{L}\mathbf{L}^\top$, the infinitesimal generator takes the following form:

$$\mathcal{L}f = -\langle \mathbf{F}\mathbf{x}, \nabla f \rangle + \langle \nabla, \mathbf{G}\nabla f \rangle \quad (25)$$

The carré-du-champ operator yields

$$\Gamma(f, g) = \nabla f^\top \mathbf{G} \nabla g = \frac{1}{2} \langle \mathbf{L}^\top \nabla f, \mathbf{L}^\top \nabla g \rangle.$$

It is worth noting that the above two operators apply to BM despite BM not having a “stationary measure”. In fact, the Lebesgue integration by parts can be illustrated using the Dirichlet operator and the self-adjointness of the BM:

$$\mathcal{E}(f, g) = \int \langle \nabla f(\mathbf{x}), \nabla g(\mathbf{x}) \rangle d\mathbf{x} = - \int f \mathcal{L}g d\pi(\mathbf{x}) = - \int f \Delta g d\mathbf{x}$$

A.3 The Spectrum of \mathcal{L}

Generalizing to forward processes of the form (22) requires working with their eigenfunctions, which can be more complicated than polynomials and may not have a closed form in general. Yet many of the results we presented for the OU process in the main text continue to hold.

The absence of a finite stationary measure for BM introduces some technicalities. The spectrum of the BM generator $\mathcal{L}f(\mathbf{x}) = \Delta f(\mathbf{x})$ contains trigonometric functions as opposed to polynomials – it is easy to verify that $\Delta e^{\nu \tau x} = \tau^2 e^{\nu \tau x}$. The orthogonal series decomposition thus breaks down for BM, as $e^{\nu \tau x}$ are not square integrable w.r.t. the Lebesgue measure. However, the ability to adequately capture the spectrum of the Laplace operator is arguably unnecessary: unlike well-defined LTI processes with finite stationary measures, the variance exploding property dictates that long-time solution ρ_T to the probability flow ODE (3) resembles a Gaussian with a large variance, and we may work with this Gaussian *in lieu* of the Lebesgue measure $d\mathbf{x}$. We can thus introduce a parametrization with $\mathbf{F} = -\epsilon \mathbf{I}$ with a small ϵ as a pragmatic approximation to BM.

For an LTI forward process with a stationary measure $\mathcal{N}(\mathbf{0}, \Sigma_\infty)$, the spectrum of \mathcal{L} closely resembles that of OU, as they consist of discrete eigenvalues in $(-\infty, -1/C] \cup \{0\}$ for some $C > 0^4$ and polynomial eigenfunctions. It is difficult to describe the exact polynomials without making major simplifications: for example, the spectrum of a one-dimensional LTI generator contains $(-c_1 n, c_2 \text{He}_n(\beta x))$ eigenpairs, where the linear multiplying constants are determined by the LTI coefficients. Section 4.10 of Bakry et al. (2013) discusses the general conditions for a discrete spectrum.

However, simply deducing that \mathcal{L} has a discrete spectrum consisting of polynomials leads to most insights discussed in this work. For example, we can similarly obtain a density ratio estimator $\check{\rho}_0/\pi$ and extend that to noise-perturbed densities using P_t , as the exponential convergence of density estimators (17) becomes

$$\left\| P_t \frac{\check{\rho}_0}{\pi} - \frac{\rho_t}{\pi} \right\|_{L^2(\pi)} \leq e^{-t/C} \left\| \frac{\check{\rho}_0}{\pi} - \frac{\rho_0}{\pi} \right\|_{L^2(\pi)},$$

where C coincides with the spectral gap parameter. Similar to the linear score estimator (20), we can construct a linear estimator in this general setting

$$\hat{\mathbf{s}}_t(\mathbf{x}) = - \left(\mathbf{A}_t \widehat{\Sigma} \mathbf{A}_t^\top + \Sigma_t \right)^{-1} (\mathbf{x} - \mathbf{A}_t \widehat{\boldsymbol{\mu}}) + \Sigma_\infty^{-1} \mathbf{x},$$

where $\widehat{\boldsymbol{\mu}}$ and $\widehat{\Sigma}$ are again the sample mean and variance of the training dataset.

A.4 Riemmanian Kernel Smoothing and Operator Score Matching

The derivation with respect to the LTI forward processes yields an approximation for Riemannian kernel smoothing (19). When t is small, we can view $\Lambda(\cdot)$ as locally constant, rendering (19) a special case of (23) with $\mathbf{F} = -\Lambda(\mathbf{x})$, $\mathbf{L} = \sqrt{2\Lambda(\mathbf{x})}$. Given an eigenvalue decomposition of $\Lambda(\mathbf{x})$, the Markov semigroup $P_t k_{s;\Lambda}(\mathbf{x}, \tilde{\mathbf{x}})$ can then be analytically computed.

A.5 Additional Notes on Hermite Polynomials

Here we recall a useful property of Hermite polynomials which facilitates higher-order score approximation for the OU process as described in Section 4. The property that we exploit is a recurrence relation for the probabilist’s Hermite polynomials, which is initialized with $\text{He}_0(x) = 1$, $\text{He}_1(x) = x$, and then follows

$$\text{He}_{n+1}(x) = x \text{He}_n(x) - n \text{He}_{n-1}(x).$$

⁴A lower bound on the nonzero eigenvalues of $-\mathcal{L}$ (often known as the *spectral gap*) is instrumental in deriving Poincaré inequalities, as well as the exponentially decaying error below; see Chapter 4 in Bakry et al. (2013).

Based on this recurrence relation, it is straight forward to recursively obtain the polynomial coefficients of each He_n , which we denote as $\text{He}_i(x) = \sum_{m=0}^i q_m^{(i)} x^m$. Now, given an arbitrary polynomial $f(x; \mathbf{p}) := \sum_{m=0}^n p_m x^m$, the task that we need to address is how to obtain the coefficients \mathbf{r} of the Hermite series $f(x; \mathbf{p}) = \sum_{m=0}^n r_m \text{He}_m(x)$. This task can be solved by observing that \mathbf{r} satisfies the linear system

$$\begin{pmatrix} \mathbf{q}^{(0)} & \mathbf{q}^{(1)} & \dots & \mathbf{q}^{(n)} \end{pmatrix} \mathbf{r} = \mathbf{p}.$$

This approach can be used to express products $\phi_i \phi_j$ of eigenvalues of the OU process as sums of individual ϕ_i , as explained in the main text.

B Further Consequences of Markov Diffusion Operators

The aim of this appendix is to revisit objectives related to score matching through the lens of Markov diffusion operators, specifically Tweedie’s formula (Tweedie, 1947), time score matching (Choi et al., 2022), and the score FPE (Lai et al., 2023b).

Insight into Tweedie’s formula Tweedie’s formula (Tweedie, 1947; Robbins, 1956; Efron, 2011) translates the task of estimating the score function $\nabla \log \rho_t(\mathbf{x})$ into the task of estimating the conditional expectation $\mathbb{E}[\mathbf{X}_0 | \mathbf{X}_t = \mathbf{x}]$. Following a similar logic to (13), we can derive an $L^2(\rho_t)$ objective for training an approximation $\mathbf{g}_t(\mathbf{x})$ to the conditional expectation as

$$\mathbb{E}_{\mathbf{X}_t \sim \rho_t} \|\mathbf{g}_t(\mathbf{X}_t) - \mathbb{E}[\mathbf{X}_0 | \mathbf{X}_t]\|^2 = \mathbb{E}_{\mathbf{X}_0 \sim \rho_0} \left(P_t \|\mathbf{g}_t(\mathbf{X}_0)\|^2 - 2\langle \mathbf{X}_0, P_t \mathbf{g}_t(\mathbf{X}_0) \rangle \right).$$

This representation disentangles the t and \mathbf{x} dependencies in the noise-perturbed distribution $\rho_t(\mathbf{x})$. Such a representation may be useful; for example, Section 4 illustrates a closed-form solution when the perturbed score is optimized within a finite subspace spanned by the eigenvectors of P_t . As another example, one could potentially construct importance sampling estimators of $P_t f$ based on other noise perturbed samples, i.e.,

$$P_t f = \mathbb{E}_{\tilde{\mathbf{x}} \sim \rho_s(\tilde{\mathbf{x}} | \mathbf{x})} \frac{f(\tilde{\mathbf{x}}) k_t(\mathbf{x}, \tilde{\mathbf{x}})}{k_s(\mathbf{x}, \tilde{\mathbf{x}})}.$$

Though we did not pursue these directions, they may be interesting to explore in future work.

Insight into time score matching An alternative to the score matching objective is to match the time derivative of the log density ratio, an approach termed *time score matching* in Choi et al. (2022). Here we point out that time score matching can be formulated in an analogous manner to (13) using the Markov semigroup, using the identity

$$\mathbb{E}_{\mathbf{X} \sim \rho_t} \left(\frac{\partial}{\partial t} f_t(\mathbf{X}) - \frac{\partial}{\partial t} \log \frac{\rho_t}{\pi}(\mathbf{X}) \right)^2 \stackrel{+C}{=} \mathbb{E}_{\mathbf{X}_0 \sim \rho_0} P_t \left(\left(\frac{\partial}{\partial t} f_t(\mathbf{X}_0) \right)^2 - 2\mathcal{L} \frac{\partial}{\partial t} f_t(\mathbf{X}_0) \right).$$

The above formula is obtained by exploiting self-adjointness of \mathcal{L} . Namely,

$$\begin{aligned} \int \left[\frac{\partial}{\partial t} f_t(\mathbf{X}) \right] \left[\frac{\partial}{\partial t} \log \frac{\rho_t}{\pi}(\mathbf{X}) \right] d\rho_t(\mathbf{X}) &= \int \left[\frac{\partial}{\partial t} f_t(\mathbf{X}) \right] \left[\frac{\partial}{\partial t} \frac{\rho_t}{\pi}(\mathbf{X}) \right] d\pi(\mathbf{X}) \\ &= \int \left[\frac{\partial}{\partial t} f_t(\mathbf{X}) \right] \mathcal{L} \left[\frac{\rho_t}{\pi}(\mathbf{X}) \right] d\pi(\mathbf{X}) = \int \mathcal{L} \left[\frac{\partial}{\partial t} f_t(\mathbf{X}) \right] d\rho_t(\mathbf{X}). \end{aligned}$$

Time score matching and score matching optimize the temporal and spatial partial derivatives of the forward process. We showcase that the process of removing intractability from the original mean squared error form follows a similar pattern. We also obtain a notably different solution compared to Choi et al. (2022).

Generalizing the score Fokker–Planck equation Sharing a similar starting point to this work, Lai et al. (2023a) noted that score matching is ambivalent to the specific forward process that is employed. The authors reasoned that the true score function ought itself to satisfy a partial differential equation (PDE) and derived an explicit PDE in the case of a Markov diffusion forward process. Here we present a streamlined and more general derivation of that result. Our main tool is the *diffusion property* of the generator \mathcal{L} which states that, for $\psi : \mathbb{R} \rightarrow \mathbb{R}$,

$$\mathcal{L}\psi(f) = \psi'(f)\mathcal{L}f + \psi''(f)\Gamma(f, f). \quad (26)$$

The diffusion property enables us to study the time evolution of the density ratio ρ_t/π , and from (7) we have that

$$\frac{\partial}{\partial t} \log \frac{\rho_t}{\pi}(\mathbf{x}) = \frac{\frac{\partial}{\partial t} P_t \frac{\rho_0}{\pi}(\mathbf{x})}{\frac{\rho_t}{\pi}(\mathbf{x})} = \log' \left(\frac{\rho_t}{\pi}(\mathbf{x}) \right) \cdot \mathcal{L} \frac{\rho_t}{\pi}(\mathbf{x}) = \mathcal{L} \log \frac{\rho_t}{\pi}(\mathbf{x}) + \left\| \nabla_{\mathbf{x}} \log \frac{\rho_t}{\pi}(\mathbf{x}) \right\|^2 \quad (27)$$

where the final equality follows from (26) with $\psi(f) = \log(f)$ and the explicit form of the carré-du-champ operator for the OU process in Example 4. The time derivative of the true score function $\mathbf{s}_t^*(\mathbf{x})$ in (9) can be obtained by taking the \mathbf{x} derivative of (27), leading in the case of the OU process to the PDE

$$\frac{\partial}{\partial t} \mathbf{s}_t^*(\mathbf{x}) = \nabla_{\mathbf{x}} [\langle -\mathbf{x}, \mathbf{s}_t^*(\mathbf{x}) \rangle + \text{tr}(\mathbf{J}(\mathbf{s}_t^*(\mathbf{x})))] + 2\mathbf{J}(\mathbf{s}_t^*(\mathbf{x}))\mathbf{s}_t^*(\mathbf{x}) \quad (28)$$

where $\mathbf{J}(\mathbf{s}_t^*)$ denotes the Jacobean of \mathbf{s}_t^* , which recovers the *score Fokker–Planck equation* as coined by Lai et al. (2023a). In that work the authors noted that standard score matching typically violates (28), especially for small values of t where the regularity of ρ_t/π is most pronounced (c.f. Fig. 1 in Lai et al., 2023a). Based on this observation, the authors proposed to add a regularization term to the score matching objective that aims to explicitly enforce (28) to (approximately) hold. The derivation that we have presented generalizes beyond the OU process by substituting alternative expressions for the infinitesimal generator and the carré-du-champ operator.

C Related Work on Orthogonal Series for Density Ratio Estimation

This appendix contains short descriptions of related work from the domains of density ratio estimation (Appendix C.1) and orthogonal series density ratio estimation (Appendix C.2). Though these works do not address DM, the insights obtained by earlier authors are relevant to the development of our proposed Riemannian DKS in Section 3 of the main text.

C.1 Density Ratio Estimation

As the ratio between two probability densities appears throughout the paper, we note that Sugiyama et al. (2012) explore this topic in great detail, albeit in an altered setting where both densities are represented by i.i.d. samples.

Notably, density ratio estimation has similarly sparked interest in a continuous interpolation between two distributions. Rhodes et al. (2020) address the difficulty of evaluating the ratio of two distributions with little overlap in support, and suggest learning the ratios of a finite interpolating sequence. Choi et al. (2022) further generalize this concept to continuous time, and develop integration by parts formula suitable for optimization. Our derivation sheds further light on density ratio estimation, contributing a simplified derivation for evaluating density ratios when the interpolation is driven by a Markovian diffusion.

C.2 Orthogonal Series Density Ratio Estimation

Density estimators based on approximation using a finite subset of orthogonal basis functions are often referred to as *orthogonal series density estimators* (Whittle, 1958; Watson, 1969; Efromovich, 2013), and we briefly discuss these in the density ratio estimation context, where they take the form

$$\frac{\tilde{\rho}_0}{\pi} = \sum_{n=1}^N \tilde{\alpha}_n \varphi_n.$$

Unlike the “soft” truncation with infinitely many nonzero terms enforced by Botev et al. (2010), setting a hard cutoff leads to negative-valued density estimates; methods to correct such irregularities were proposed in Glad et al. (2003). Estimating each coefficient $\tilde{\alpha}_n$ using the empirical mean leads to undersmoothed density estimation, similar to the Stein effect in the kernel context. Therefore, most orthogonal series estimators are *modulated* – for example, Beran and Dumbgen (1998); Beran (2000) propose modulating the empirical mean with coordinate-wise shrinkage parameters, i.e., $\tilde{\alpha}_n := w_n \hat{\alpha}_n, 0 \leq w_n \leq 1$.

D Experimental Settings: Toy Datasets

This appendix contains full details required to reproduce the two-dimensional experiments that we reported in the main text. Details for standard DM OISM are contained in Appendix D.1, details for RDKS are contained in Appendix D.2. Additional empirical results are presented in Appendix D.3.

Computational resources All toy experiments were implemented in JAX and performed on the CPU of an Apple MacBook M2 laptop. The methods take a similar amount of computational resource to run: it is easier for RDKS to perform well in this instance, meaning that a smaller number of iterations were required.

Synthetic datasets Synthetic data were generated using existing code that was downloaded from <https://github.com/rtqichen/ffjord>, under the MIT licence. For all experiments, we generated a synthetic dataset of size $N = 2,048$.

General notes on score matching implementation For both toy and MNIST experiments, we broadly followed the convention established by Ho et al. (2020). Specifically, we followed the standard practice of predicting the noise perturbation ϵ given a perturbed sample $\alpha_t \mathbf{x} + \sigma_t \epsilon$. I.e., minimizing the following squared loss equivalent to score matching (eq. 12 of Ho et al. (2020)):

$$\min_{\theta} \mathbb{E}_{\mathbf{x} \sim \rho_0, \epsilon \sim \mathcal{N}(\mathbf{0}, \mathbf{I})} \|\widehat{\epsilon}_{\theta}(\alpha_t \mathbf{x} + \sigma_t \epsilon, t) - \epsilon\|^2.$$

Under this approach $\tilde{\mathbf{x}} - \widehat{\epsilon}_{\theta}(\tilde{\mathbf{x}}, t)/\sigma_t$ corresponds to an estimate of $\nabla \log(\rho_t/\pi)(\tilde{\mathbf{x}})$.

The rest of our score matching experimental set-up similarly follows Ho et al. (2020), such as the use of the log signal-to-noise ratio as a surrogate of the time variable, and sampling from the set of perturbation using a beta schedule.

Given the equivalence between learning the $\nabla \log \rho_t/\pi$ and learning the noise perturbation $\widehat{\epsilon}$, it is straightforward to convert a linear estimator for $\widehat{\epsilon}$ into a linear estimator for $\nabla \log \rho_t/\pi$, and vice versa. The SDE-based sampling approach described in Algorithm 2 of Ho et al. (2020) was used to simulate samples presented in panel (c) of Figure 3. Adaptive ODE solvers (dopr15) were used to generate samples using probability flow ODE Equation (3) to produce column (d) of Figure 3.

D.1 Score Matching Implementation for DM and OISM

For the training the neural network in the context of both standard DM and OISM we minimized the score matching objective (13), approximated using minibatches of size 256, with 30,000 iterations of the Adam optimiser and learning rate 2×10^{-3} . Both experiments take around 154 seconds to run; there was no appreciable increase in computational cost due to employing the OISM methodology in this experiment.

For the neural network we employed a 9-layer feed-forward neural network with 32 hidden units activated by the Sigmoid Linear Unit (SiLU). The technical specifics, such as how parameters were initialised, are detailed in the code provided as electronic supplement. The neural network was used to directly model the score function in standard DM, and used as a flexible model for the residual $\mathbf{r}_t(\mathbf{x})$ in OISM, as described in Section 4 of the main text.

D.2 Riemannian Diffusion Kernel Smoother

This section contains full details on how RDKS was implemented. As described in the main text, the metric tensor was estimated as a hyperparameter defined at each data point: $\mathbf{\Lambda}_n := \mathbf{\Lambda}(\mathbf{x}_n)$. In practice we employed an eigenvalue decomposition

$$\mathbf{\Lambda}_n = \mathcal{C}(\mathbf{Q}_n) \text{diag}(\ell_n) \mathcal{C}(\mathbf{Q}_n)^{\top},$$

where \mathbf{Q}_n is a skew-symmetric matrix and \mathcal{C} denotes the Cayley transform, a bijection to the space of orthonormal matrices, i.e. $\mathcal{C}(\mathbf{Q}_n) = (\mathbf{I} - \mathbf{Q}_n)(\mathbf{I} + \mathbf{Q}_n)^{-1}$. The hyperparameters ℓ_n and \mathbf{Q}_n were then estimated.

To control computational cost, the kernel hyperparameters were trained using a standard score matching objective (12) computed on $n < N$ weighted samples from $\hat{\rho}_0$; similar to sparse kernel machines, we approximate the empirical data samples $\hat{\rho}_0$ with a weighted subset. Namely, we choose by k -means a subset $\{\tilde{\mathbf{x}}_i\}_{i=1}^n$ of training data of size $n = 256$, and endowed each sample with its own kernel hyperparameters $\check{\ell}_i$ and $\check{\mathbf{Q}}_i$. Effectively, we use the following density ratio estimator

$$\frac{\check{\rho}_t}{\pi}(\mathbf{x}) = \sum_{i=1}^n \beta_i k_t(\mathbf{x}, \tilde{\mathbf{x}}_i; \check{\ell}_i, \check{\mathbf{Q}}_i), \quad \beta_1 + \dots + \beta_n = 1.$$

It is worth noting evaluating kernel hyperparameters and the appropriate level of smoothing (denoted by the subscript t in (19)) is merged into one joint task of kernel hyperparameter estimation in practice, as we observe that adopting a new smoothing parameter t is equivalent to multiplying the lengthscale ℓ by a constant. The training of RDKS is straightforward in that the initial score solution is the memorized score: we implement 10,000 iterations with perturbed minibatches of 256 samples and an Adam learning rate of 10^{-3} . The training process usually takes 140 seconds.

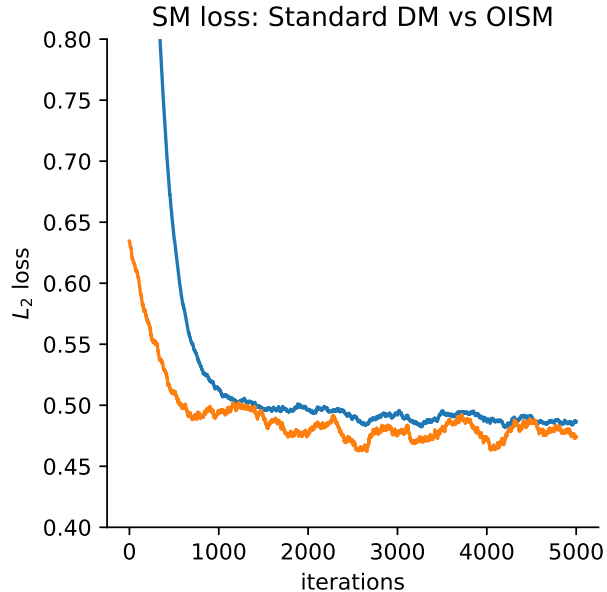


Figure 2: A comparison of the score matching loss of **standard DM** and **OISM** during training, for the experiment reported in Figure 1. The score matching loss tends to be insensitive to inaccurate density estimates, as revealed by contrasting the similar training losses in this plot with the differing performance of **standard DM** and **OISM** at density estimation in Figure 1.

D.3 Additional Results

The experimental setup that we have just described was used to produce Figure 1 in the main text. Here we additionally present Figure 2, which displays the score matching loss obtained under training of standard DM and OISM for the same experiment. The score matching loss tends to be insensitive to inaccurate density estimates, as revealed by contrasting the similar training losses in Figure 2 with the differing performance of standard DM and OISM at density estimation in Figure 1.

Further, we also provide results for a range of target distributions p_{data} in Figure 3. Similar conclusions to those drawn for Figure 1 continue to hold for the results shown in Figure 3. Namely, we observed consistent inaccuracy of the density estimates produced by standard DM (second column), and inaccurate samples simulated using the probability flow ODE (3) using standard DM (fourth column). These inaccuracies are somewhat remedied by applying the SDE-based reverse sampler method of Song and Ermon (2020) (third column) to the score approximation learned in standard DM. In contrast, the densities learned by our proposed methods, RDKS (fifth column) and OISM (last column), are in all cases accurate. In particular, accurate samples can be generated from RDKS and OISM (using the probability flow ODE) without recourse to injecting additional stochasticity into sample generation, as seems to be required for standard DM.

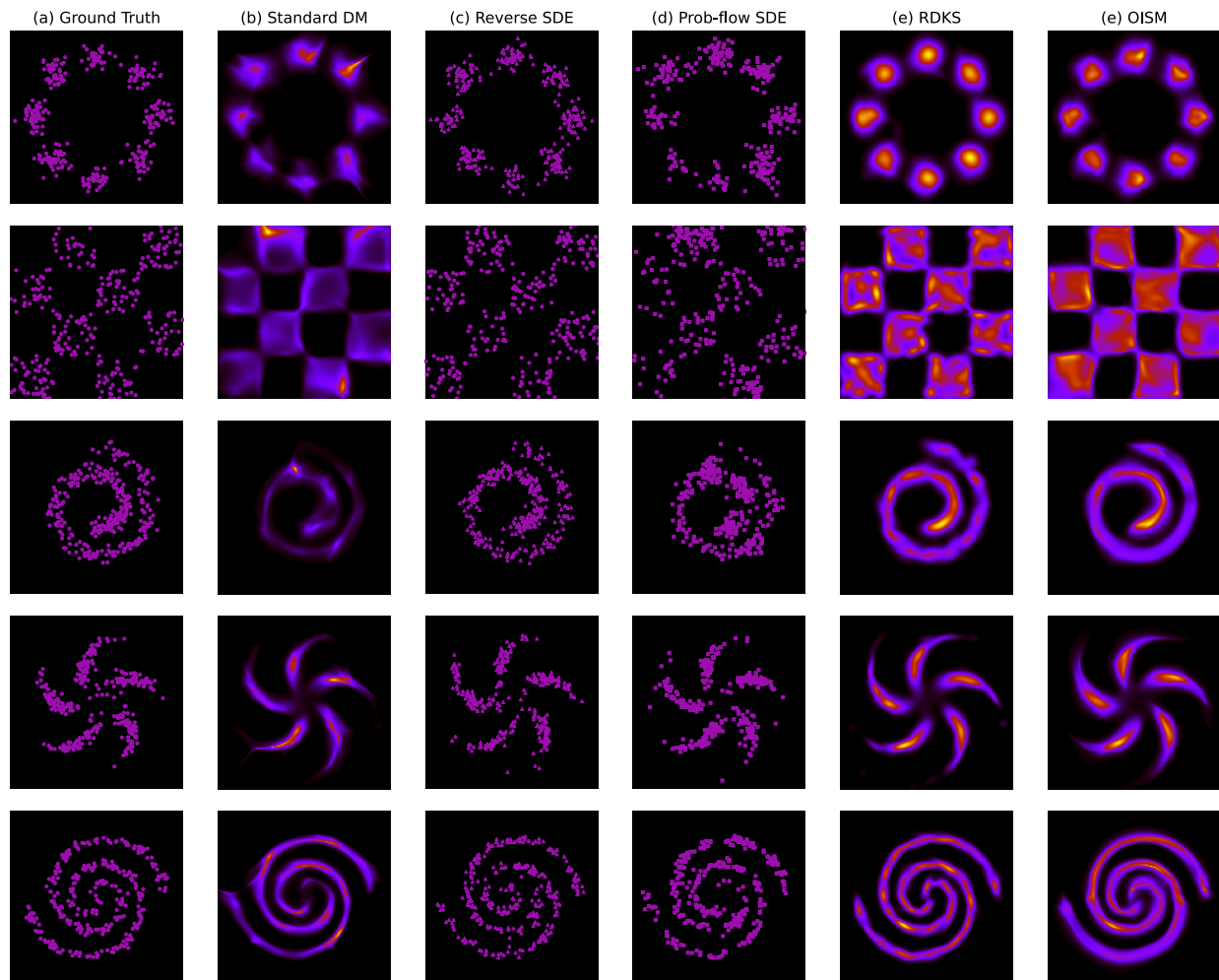


Figure 3: An empirical proof-of-concept, extended. This figure compares standard DM (Ho et al., 2020) with our two proposed methods, RDKS and OISM. The first column shows the training dataset, and each row corresponds to a generative modelling task (8 Gaussians, checkerboard, Swissroll, pinwheel and 2 spirals). Results from standard DM are shown as density estimates (second column), samples generated using the SDE-based reverse sampler of Song et al. (2020) (third column), and the probability flow ODE (3) (fourth column). Results from our methods are shown as density estimates, for RDKS (fifth column) and OISM (last column). These indicate that better density estimates are produced when the underlying properties of the Markov diffusion process are enforced.

E Experimental Settings: MNIST

This appendix contains full details required to reproduce the MNIST experiment that we reported in the main text. Details for standard DM are contained in Appendix E.1, while details for OISM are contained in Appendix E.2. Additional experimental results are presented in Appendix E.3.

Computational resources For these experiments we used a PyTorch implementation that runs remotely using an Nvidia A100 GPU.

Implementation details In addition to the model design choices described in Appendix D. We follow the PyTorch implementation of the denoising diffusion probabilistic model (Ho et al., 2020) that was downloaded under the MIT license from <https://github.com/lucidrains/denoising-diffusion-pytorch/tree/main>. The implementation is slightly modified for OISM, and we use differential equation solvers obtained from <https://github.com/rtqichen/torchdiffeq> to add an implementation of the probability flow ODE (3).

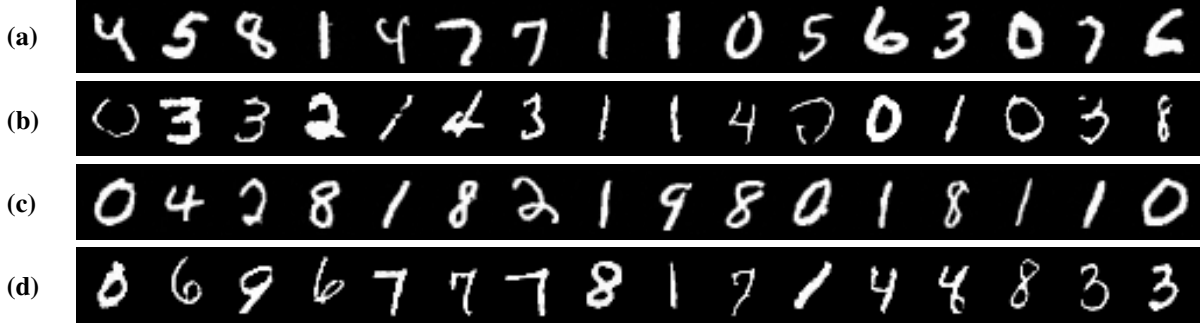


Figure 4: Illustration using MNIST: Here we showcase samples generated by standard DM ((a) and (b)) and OISM ((c) and (d)). The SDE-based stochastic sampler of Song and Ermon (2020) was used to generate (a) and (c), while the probability flow ODE was used to generate (b) and (d).

Dataset The MNIST dataset was downloaded from <http://yann.lecun.com/exdb/mnist/> under the terms of the Creative Commons Attribution-Share Alike 3.0 license. The image pixel values were normalized to a $[-1, 1]$ range for the purpose of constructing a DM.

E.1 Standard Diffusion Modelling

Following common experimental practice for image generation tasks, a UNet architecture for score estimation was used. Specifically, we adopted a UNet consisting of 3 ResNet blocks and learned time embeddings⁵. A total of 50,000 iterations of Adam were performed, with minibatch size of 256, and UNet parameters were optimized with learning rate 10^{-4} . The total running time was about 3.5 hours.

E.2 Operator-Informed Score Matching

Here we provide some brief remarks on OISM that are necessary to understand how our experiments can be reproduced. Recall that the linear score approximation $\hat{s}_t(\mathbf{x})$ provided by OISM requires that the matrices $\alpha_t^2 \hat{\Sigma} + \sigma_t^2 \mathbf{I}$ in (20) be inverted. This was achieved by first obtaining an eigendecomposition $\mathbf{V} \text{diag}(\psi) \mathbf{V}^\top$ of $\hat{\Sigma}$, yielding

$$\left(\alpha_t^2 \hat{\Sigma} + \sigma_t^2 \mathbf{I}\right)^{-1} = \mathbf{V} \text{diag}\left(\frac{1}{\alpha_t^2 \psi_d + \sigma_t^2}\right) \mathbf{V}^\top.$$

Similar to the toy experiments that we reported, here we used the UNet architecture as a flexible model for the residual $\mathbf{r}_t(\mathbf{x})$, as described in the main text.

For this experiment we ran a total of 50,000 iterations with minibatch size of 256, and UNet parameters were optimized using Adam with learning rate 2×10^{-4} – the extra linear term of OISM allowed for a higher learning rate in this experiment. The total running time was about 3.5 hours – it took negligibly longer than standard DM because the extra computation required for OISM constituted a small fraction of the overall computational cost.

E.3 Additional Results

Samples generated from both standard DM and OISM are displayed in Figure 4. It is seen in Figure 5 that the samples generated using OISM are more consistent with the range of values contained in the MNIST dataset.

⁵Full details are provided as part of the code contained in the electronic supplement.

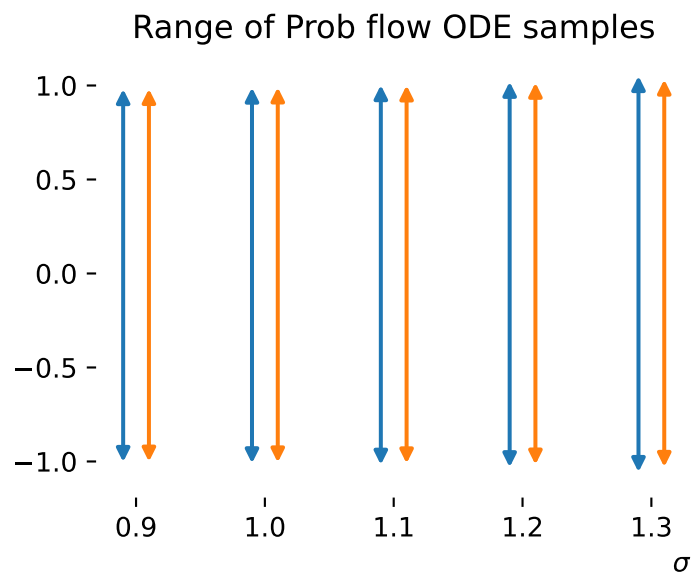


Figure 5: We illustrate that OISM can avoid the worse case scenario when the initial starting point of the probability flow ODE lies within a low density area of the standard Gaussian distribution. We simulate samples using slightly tempered initial distributions (Gaussian distributions with standard deviation σ), and see if the generated MNIST images conform to the support $[-1, 1]$. While the effect is not significant, we observe a consistent positive effect from OISM in converging towards the support of the data distribution.